Fatigue strength capacity of load-carrying fillet welds on ultra-high-strength steel plates subjected to out-of-plane bending

Ahola Antti, Björk Timo, Barsoum Zuheir

DOI: 10.1016/j.engstruct.2019.109282

Fatigue strength capacity of load-carrying fillet welds on ultra-high-strength steel plates subjected to out-of-plane bending

A. Ahola[1*], T. Björk[1], Z. Barsoum[2]

[1]School of Energy Systems, Lappeenranta-Lahti University of Technology LUT, P.O. Box 20, FI-53851 Lappeenranta, Finland

[2]Department of Aeronautical and Vehicle Engineering, KTH Royal Institute of Technology, Teknikringen 8, SE-10044 Stockholm, Sweden

ABSTRACT

Weld root fatigue strength capacity is an important design criterion in load-carrying (LC) fillet welded joints subjected to cyclic loads. This paper elaborates on the weld root fatigue strength capacity of fillet welded LC joints made of ultra-high-strength steel (UHSS) and subjected to out-of-plane bending. Experimental fatigue tests are carried out using constant amplitude loading with an applied stress ratio of R = 0.1 with both pure axial, i.e. DOB = 0 (degree of bending, bending stress divided by total stress) and bending, i.e. DOB = 1.0, load conditions. The applicability of different approaches – nominal weld stress, effective notch stress concepts, and 2D linear elastic fracture mechanics (LEFM) – for the fatigue strength assessment of weld root capacity is evaluated. Furthermore, a parametric LEFM analysis is used to evaluate the effect of weld penetration on the root fatigue strength capacity in axial and bending loading. The results indicate that in the case of bending, nominal weld stress can be calculated using the linear stress distribution over the joint section and FAT36 as a reference curve. In the bending loading, for the joints failing from the weld toe, a mean fatigue strength of up to 185 MPa in the nominal stress system was achieved, indicating that the reference curve FAT63 is overly conservative. The ENS concept with FAT225 seemed to be slightly unconservative for assessing the root fatigue strength capacity. LEFM analyses revealed that in the case of increasing weld penetration and bending loading, weld root fatigue strength capacity seemed to correlate with the nominal weld stress calculated using effective weld throat thickness, while in axial loading, weld stress should be calculated using external throat thickness summed with penetration length.

Keywords: Fatigue assessment; welded joints; weld root fatigue strength; bending; ultra-high-strength steel; load-carrying joint

[*] Corresponding author: Antti Ahola (antti.ahola@lut.fi)

1 INTRODUCTION

Lightweight structures have a reduced environmental impact as they allow a decrease in material usage, weight, and production resources used. The introduction of lightweight structures is connected to the possibility of using high-strength steel (HSS). Higher structural performance and energy efficiency of metal structures is increasingly required in many fields, such as in the automotive, construction and offshore industry. The objective to optimize structures with the minimized weight and cost, and increase thus the structural performance and energy efficiency, pose challenges for the designers and analysts. Structures made of HSS or ultra-high-strength steel (UHSS) plates incorporate typically welding, and an awareness regarding the potential failure mechanisms is also needed. One of the main challenges when using HSS to achieve lightweight design of welded structures and components is to obtain high weld quality and simultaneously, minimize the scatter of quality in manufacturing. Other important aspects are the accurate assessment of the fatigue life of welded structures and adequate concepts for these assessments. One of the critical steps in the fatigue life assessment of welded structures is the adequate determination of effective stress, which is one of the uncertainty parameters that results in a variation in the life estimation. A common engineering practice is to consider the most conservative approach, which often leads to unnecessarily over dimensioned welded joints and structures.

Weld root fatigue strength capacity, due to unpenetrated weld or insufficient throat thickness, is an essential design criterion in load-carrying (LC) joints. Depending on the weld size and its location, the share of secondary bending stresses at the adjoined plate member, and potentially conducted post-weld treatments, a fatigue crack may initiate from the weld toe or the weld root [1–3]. Fatigue strength capacity of the weld root can be assessed using stress-based approaches, i.e. nominal stress, hot spot (HS) stress or effective notch stress (ENS) or using fracture mechanics and crack propagation analysis. Of these, the nominal stress method is the most elementary of the fatigue assessment approaches. In a pure axial loading, the nominal weld stress (NWS) range $\Delta\sigma_w$ is calculated at the shortest ligament of the weld, usually corresponding to throat thickness, and fatigue life is obtained using characteristic reference curve FAT36 [4–6].

For LC joints with throat bending, structural weld stress methods have been established. Fricke *et al.* [7] proposed a method that is based on the structural stress at the weld leg length following the failure path of the root failure. Alternatively, structural stress can be calculated at the throat section following the procedure proposed by Sørensen *et al.* [8]. However, these methods have not been officially included in the design codes and guidelines, and are thus not the focus of this study. In more complex structural components, the ENS concept can be applied for the fatigue assessment of the weld root using the reference radius r_{ref} = 1.00 mm and the

reference curve FAT225 or FAT200 for the maximum principal or von Mises stress criterion, respectively [9]. Recently, Sundermeyer *et al.* [10] analyzed and tested partially and fully penetrated single-sided welded thick-walled T-joints (t = 24.5 mm), indicating that the increasing penetration depth improved the fatigue strength of the weld root in terms of the ENS system. In the partially penetrated joints with an initial crack due to an infusible weld root face, FAT225 appeared to be unconservative. This issue was also previously reported by Fricke and Kahl [11] for fillet welded hollow sections with an end or intermediate plate. In their studies, the fatigue test results barely exceeded the FAT225 reference curve.

Due to the insidious characteristics of root side failures, i.e. the fact that the failure cannot be visually monitored until the crack has propagated through the weld or parent material, the fatigue strength properties of LC joints have been comprehensively investigated in recent decades. Also, different load conditions, such as shear loading and multiaxial loads, have come under investigation. Kim *et al.* [12] studied the effect of the direction of uniaxial loading, i.e. the share of shear load component, on the fatigue capacity of LC joints. Khurshid *et al.* [13] and Frendo and Bertini [14] investigated tubular joints subjected to multiaxial loads. However, the vast majority of previous experimental studies [15] have focused on single- or double-sided fillet welds where the adjoined plate member is subjected to axial membrane loading having only secondary bending due to the angular distortion or the axial offset of adjoined plate members, as in [16] . Supposedly, there are two main reasons for this: Firstly, the root fatigue capacity of double-sided fillet welded joints subjected to bending is much higher than joint subjected under axial tension and consequently, careful consideration of potential root fatigue is particularly required in the case of axial loading [17–19]. Secondly, due to complexity of bending test procedure, axial tension tests have been preferred [20].

The existence of bending stresses induced by external bending loading, axial misalignment or angular distortion in an adjoined plate member, see Fig. 1, cannot totally be neglected and should be taken into account in fatigue strength assessment. Moreover, current design codes do not give instructions for the consideration of bending stresses in the weld root fatigue strength assessment of double-sided fillet welded joints. Fatigue strength properties of non-load carrying joints made of HSS or UHSS have been widely studied in recent years but less attention has been paid to the root fatigue strength properties of strength-matching weld metals.

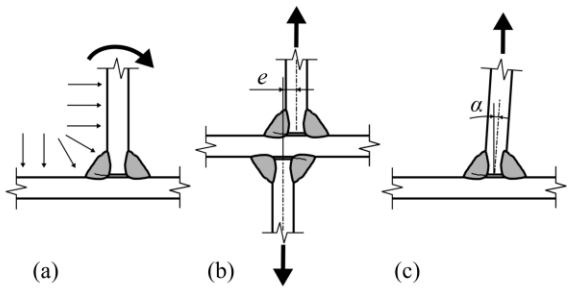

Fig. 1. Fillet welded LC joints where bending stresses are induced by: (a) external bending loading or structural discontinuity, (b) plate axial offset, and (c) angular misalignment.

This paper evaluates the root side fatigue strength capacity of double-sided fillet welded LC joints made of UHSS. Experimental fatigue tests were carried out using constant amplitude loading with an applied stress ratio of R = 0.1. The focus of this paper is on DOB = 1.0 (degree of bending, bending stress divided by total stress) out-of-plane loading but DOB = 0 axial loading was also considered to have a reasonable comparison between different load conditions. Hereby, an analytical fatigue assessment procedure for the calculation of the weld root stresses under bending loading is proposed. Furthermore, the paper discusses the applicability of the ENS approach and two-dimensional linear elastic fracture mechanics (LEFM) for the fatigue assessment of root side failures and the effect of weld penetration on the root side fatigue strength capacity of double-side fillet welded joints.

2 EXPERIMENTAL PROGRAM

2.1 Materials

Experimental fatigue tests were carried out for LC joints made of direct-quenched S960 MC sheet metals. With the direct-quenching, high mechanical properties can be obtained with the minimized need for the alloying. Böhler Union X96 (Ø1.0 mm), which is a strength-matching filler material for S960 steels, was used in the preparation of the test specimens. The chemical compositions and mechanical properties of the base and filler materials are presented in Table 1 and Table 2, respectively. In Tables 1-2, the measured items represent the values obtained from the material certificate provided by the material supplier.

Table 1. Chemical compositions of the studied materials [weight-%].

Material	Type	C	Si	Mn	P	S	Cr	Ni	Mo	Cu	Nb	N
S960 MC	maximum	0.12	0.25	1.30	0.02	0.01						
	measured	0.097	0.20	1.09	0.008	0.001	1.13	0.38	0.191	0.033	0.001	0.005
Union X96	nominal*	0.12	0.8	1.9			0.45	2.35	0.55			

* Undiluted weld metal

Table 2. Mechanical properties of the studied materials.

Material	Type	Proof strength $R_{p0.2}$ [MPa]	Ultimate strength R_m [MPa]	Ultimate elongation A [%]	Min. impact toughness KVC [J]
S960 MC	nominal	960	980-1250	7	27 (-40°C)
	measured	1041	1210	11	65 (-40°C)
Union X96	nominal	930	980	14	80 (+20°C) 47 (-50°C)

2.2 Test specimens

Load carrying fillet welded joints were fabricated of t = 9 mm S960 MC plates using a gas metal arc welding (GMAW) process (135) [21] and a welding robot to achieve a uniform metallurgical quality and weld reinforcement geometry. Two types of test specimens were fabricated: For the axial (DOB = 0) tests, specimens with widenings for clamping, Fig. 2a, and for the bending (DOB = 1.0) tests, specimens with a uniform width, Fig. 2b, were fabricated. Due to the high weld root fatigue capacity of bending loaded joints, small throat thicknesses were preferred and a = 4 mm throat thickness was solely pursued within these joints. In the axially loaded joints, the weld root is more critical than weld toe and consequently, both a = 4 mm and a = 5 mm target throat thicknesses were manufactured and tested; see Table 4. In two specimens (FWB_DYN7 and FWB_DYN8), double beveling was used to test the effect of weld penetration and reinforcement location on the fatigue strength capacity. In the other specimens, no groove preparation was conducted. The main welding parameters are presented in Table 3 for the two different throat thicknesses. The realized values are presented in Table 4.

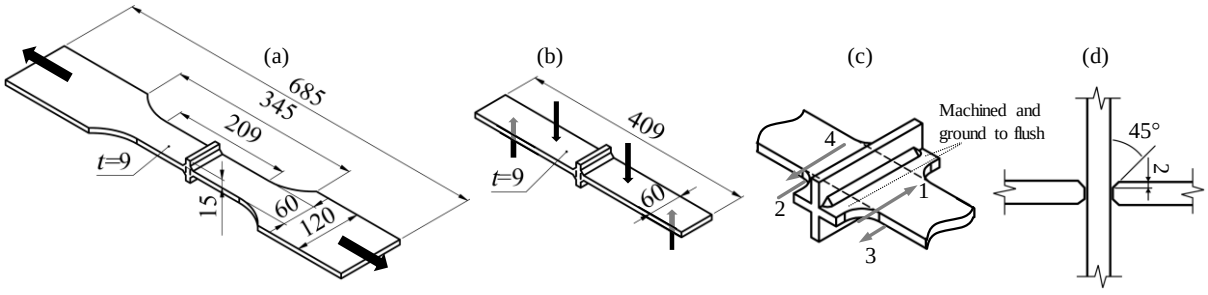

Fig. 2. Shape (after removing weld run-on and run-off parts) and dimensions of the test specimens: (a) axially and (b) bending loaded LC joints; (c) sequence of welds and preparation of the specimens; and (d) partial K-groove preparation used in the FWB_DYN7 and FWB_DYN8 specimens (all dimensions in mm).

Table 3. Welding parameters for the different target throat thicknesses (a_{target}): average value measured for each pass and the corresponding standard deviations (stdv). Heat input Q calculated according to EN 1011-1 [22] using a thermal efficiency of k = 0.8 for the GMAW process.

a_{target} [mm]	Pass ID	Type	Current I [A]	Voltage U [V]	Travel speed v [mm/s]	Wire feed rate w [m/min]	Heat input Q [kJ/mm]
4	1-4	average	233	27.6	9.5	13.2	0.54
4		stdv	1.4	0.15	*	*	$3.2 \cdot 10^{-3}$
5	1-4	average	232	28.3	5.9	13.2	0.90
5		stdv	0.76	0.11	*	*	$3.1 \cdot 10^{-3}$

* Pre-set constant value for the welding robot, no variation

Preliminary tests, conducted for joints in AW condition and subjected to a DOB = 1 loading, indicated that the weld root fatigue capacity was substantially higher than the weld toe, resulting in fatigue failures from the weld toe, see Table 5 in Section 2.4. Consequently, high frequency mechanical impact (HFMI) treatment was employed at the weld toe in the remaining specimens to achieve a fatigue failure from the weld root. The HFMI treatment resulted in improved weld toe geometry in terms of a higher toe radius and beneficial compressive residual stresses; see Fig. 3. Plate surface normal residual stresses parallel to the loading direction were measured using an X-ray diffractometer (Stresstech Xstress G3000) in the selected specimens representing the test series. Table 4 presents the test matrix and conducted procedures for each specimen. In Table 4, n/a refers to not relevant for the specimens failing from the weld toe.

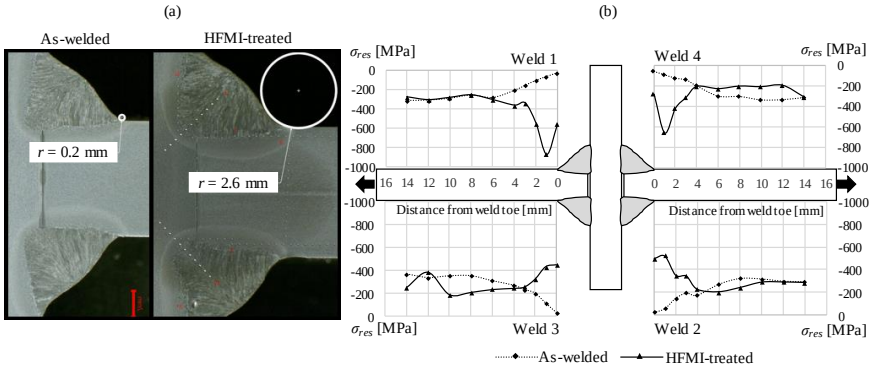

Fig. 3. (a) Weld toe geometry; (b) surface residual stress distribution along specimen surface in as-welded and HFMI-treated conditions.

Table 4. Test matrix and weld reinforcement geometry. a_1 and a_2 are the throat thicknesses of the failed weld pair (the welds 1 and 3, or the welds 2 and 4; see Fig. 2c), $a_{i,eff}$ is the corresponding effective throat thickness calculated considering the weld penetration, w is the width of the non-fused weld root, and ΔM_{exp} and ΔF_{exp} are the experimental test moment and force, respectively. AW signifies the as-welded condition.

Specimen ID	Load type A = axial B = bending	Test condition	Groove preparation	a_1	a_2	$a_{1,eff}$	$a_{2,eff}$	w	ΔM_{exp}	ΔF_{exp}
				[mm]					[Nm]	[kN]
FWB_DYN1	B	AW	-	3.7	3.7	n/a	n/a	n/a	278	-
FWB_DYN2	B	AW	-	3.4	3.4	n/a	n/a	n/a	263	-
FWB_DYN3	B	AW	-	3.8	3.8	n/a	n/a	n/a	223	-
FWB_DYN4	B	HFMI	-	n/a	n/a	n/a	n/a	n/a	306	-
FWB_DYN5	B	HFMI	-	4.0	4.1	4.9	4.9	6.7	371	-
FWB_DYN6	B	HFMI	-	4.1	4	4.8	4.7	7.0	412	-
FWB_DYN7	B	AW	Partial K	3.2	3.2	n/a	n/a	n/a	344	-
FWB_DYN8	B	AW	Partial K	3.6	3.6	n/a	n/a	n/a	257	-
FWB_DYN9	B	HFMI	-	4.0	4.2	4.8	4.9	6.8	512	-
FWB_DYN10	B	HFMI	-	4.1	3.9	4.9	4.8	6.6	430	-
FWB_DYN11	B	HFMI	-	4.2	4	5	4.8	6.7	485	-
FWB_DYN12	B	HFMI	-	3.8	3.7	4.6	4.5	6.7	548	-
FWB_DYN13	B	HFMI	-	n/a	n/a	n/a	n/a	n/a	439	-
FWB_DYN14	A	HFMI	-	4.2	4	4.8	4.6	7.2	-	81.6
FWB_DYN15	A	HFMI	-	3.9	4.3	4.6	5.1	6.9	-	55.3
FWB_DYN16	A	HFMI	-	4.5	5.1	5	5.5	7.7	-	73.2
FWB_DYN17	A	HFMI	-	4.7	5.3	5.2	5.7	7.7	-	64.2

2.3 Test set-up

For joints subjected to out-of-plane bending, a four-point bending device producing a constant bending moment with no shear stress between the inner press rolls was assembled; see Fig. 4b. For joints subjected to axial loading, a conventional test rig, whereby the specimen is clamped to jaws, was used; see Fig 4a. In both test set-ups, the force was produced using a servo-hydraulic cylinder. During tests, the minimum and maximum of applied load and displacements were recorded. Despite almost nonexistent secondary bending stresses due to the straightness of specimens and the loading type in the case of bending, each specimen was instrumented with a strain gage at a $0.4t$ = 3.6 mm distance from the weld toe. The failure criterion for the end of a test was a fracture of the specimen.

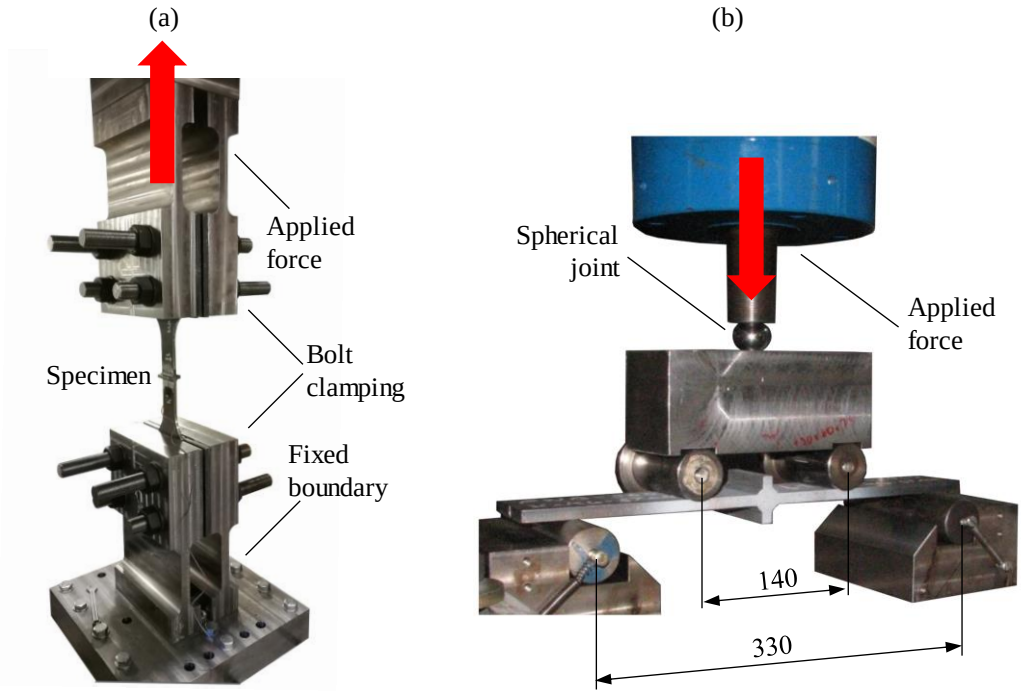

Fig. 4. Test set-ups: (a) axial and (b) bending tests.

2.4 Results

Table 5 presents the fatigue test results for all tested joints. In the axially loaded specimens that failed from the weld root, the weld stress range is calculated for the gross weld area according to the design codes [4–6,23] as follows:

$$\Delta\sigma_w = \frac{t}{2a_{eff}}\Delta\sigma, \tag{1}$$

where t is the plate thickness, a_{eff} is the effective throat thickness (considering the weld penetration; see Table 4) and $\Delta\sigma$ is the maximum nominal stress at the adjoined plate component; see Fig. 5. Respectively, for the bending loaded specimens, an elastic stress distribution in the gross cross section of the weld areas, as this paper proposes, was assumed. A similar concept regarding elastic stress distribution for single-sided welds has been applied previously by Sundermeyer *et al.* [10]. By adopting this concept concerning the reference weld root stress in bending loading, for double-sided fillet welded joints, the corresponding elastic stress range at the weld root is:

$$\Delta\sigma_w = \frac{\Delta Mc}{I} = \frac{\frac{\Delta\sigma t^2}{6}\frac{w}{2}}{\frac{(w+2a_{eff})^3 - w^3}{12}} = \frac{\Delta\sigma t^2 w}{6a_{eff}w^2 + 12wa_{eff}^{\ 2} + 8a_{eff}^{\ 3}}, \tag{2}$$

where ΔM is the moment range acting on the adjoined plate component, I is the second moment of area, w is the width of the non-fused weld root and c is the distance from the neutral axis to the weld root ($c = w/2$ in the case of symmetric welds); see Fig. 5.

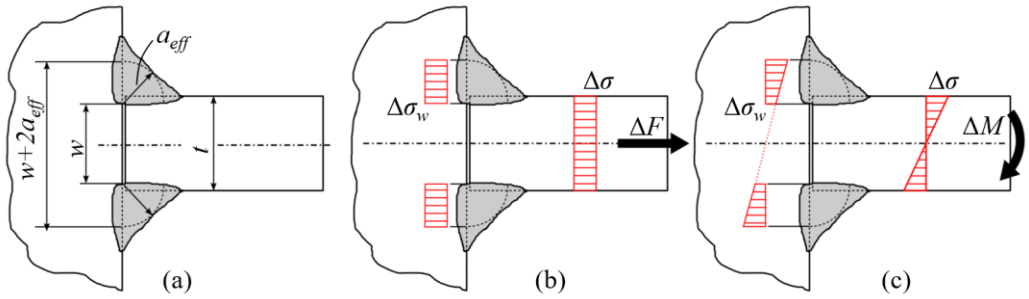

Fig. 5. (a) Dimensions of LC joints, and weld stresses for (b) axially and (c) bending loaded specimens in terms of the nominal stress system.

In both loading types, the penetration obtained by macro graphic investigations, see Fig. 8 and Table 4, was included in the calculation of the root stress to obtain more conservative results. Only the specimens with an observable failure from weld root (WR) were considered in the calculation of the root fatigue strength; see Table 5. The joints failing from the weld toe, i.e. the AW joints FWB_DYN1-3 and FWB_DYN7-8, were included in the analysis of the weld toe fatigue strength, respectively. The test results of the FWB_DYN4 and FWB_DYN13 specimens were excluded from further analysis since they failed from the base material. For the ENS system, 2D FEA was employed to obtain SCF $k_t(r_{ref} = 1$ mm) values, and to convert nominal plate stress to ENS at weld root or weld toe depending on the failure location. A more detailed description of the FE modeling can be found in Section 3.

Table 5. Fatigue test results.

Specimen ID	Loading type A = axial B = bending	$\Delta\sigma$ [MPa]	$\Delta\sigma_w$ [MPa] Eqs (1-2)	$\Delta\sigma_{ens}$ [MPa]	N_f [10^3 cycles]	Failure location WR = weld root WT = weld toe BM = base material
FWB_DYN1	B	344	n/a	660	192	WT
FWB_DYN2	B	325	n/a	632	343	WT
FWB_DYN3	B	275	n/a	528	1 163	WT
FWB_DYN4	B	378	n/a	n/a	946	BM
FWB_DYN5	B	458	60	334	774	WR
FWB_DYN6	B	509	69	392	556	WR
FWB_DYN7	B	424	n/a	809	128	WT
FWB_DYN8	B	317	n/a	599	486	WT
FWB_DYN9	B	632	84	461	324	WR

FWB_DYN10	B	531	70	393	557	WR
FWB_DYN11	B	599	78	454	506	WR→WT+BM
FWB_DYN12	B	676	102	547	229	WR→BM
FWB_DYN13	B	542	n/a	n/a	418	BM
FWB_DYN14	A	153	145	593	120	WR
FWB_DYN15	A	103	95	395	320	WR
FWB_DYN16	A	136	117	536	206	WR
FWB_DYN17	A	119	99	461	290	WR

The mean fatigue strength for each approach, was calculated using the standard procedure according to the IIW Recommendations [4], i.e. stress as an independent variable and fatigue life as the dependent variable. In the joints failing from the weld root, only the fixed slope of the S-N curve (m = 3) was used in the fatigue strength assessment; see Fig. 6. For the weld root failures, the FAT36 characteristic design curve following the IIW Recommendations [4] and EC3 [5] was chosen for a comparison.

The test results of the joints with a toe failure indicated that a shallower slope would fit the test data more comprehensively, and consequently, both m = free and m = 3 regression analyses were conducted; see Fig. 7. No distinct improvement, however, was found in the joints with partial K-groove preparation with regard to purely fillet welded joints; see Fig. 7. For that reason, all weld toe failure test results were included in the same regression analysis. In the case of bending loading, it must be considered that no secondary bending stress is induced by the angular distortion, and the nominal stress is thus equal to the structural hot spot stress.

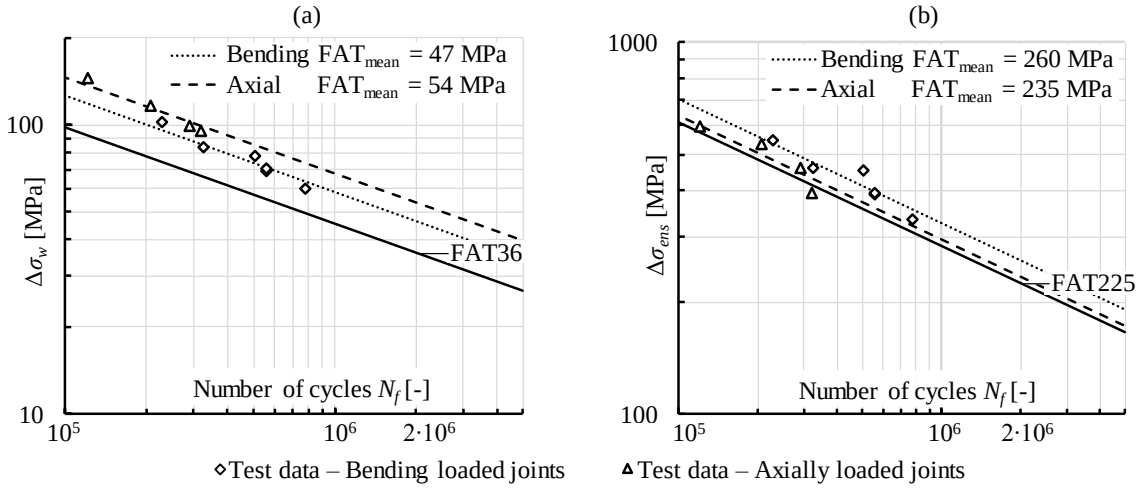

Fig. 6. Fatigue test results for joints with root failure and the derived S-N curves in terms of (a) the NWS and (b) ENS system. The slope of the S-N curve m = 3 is used in all cases.

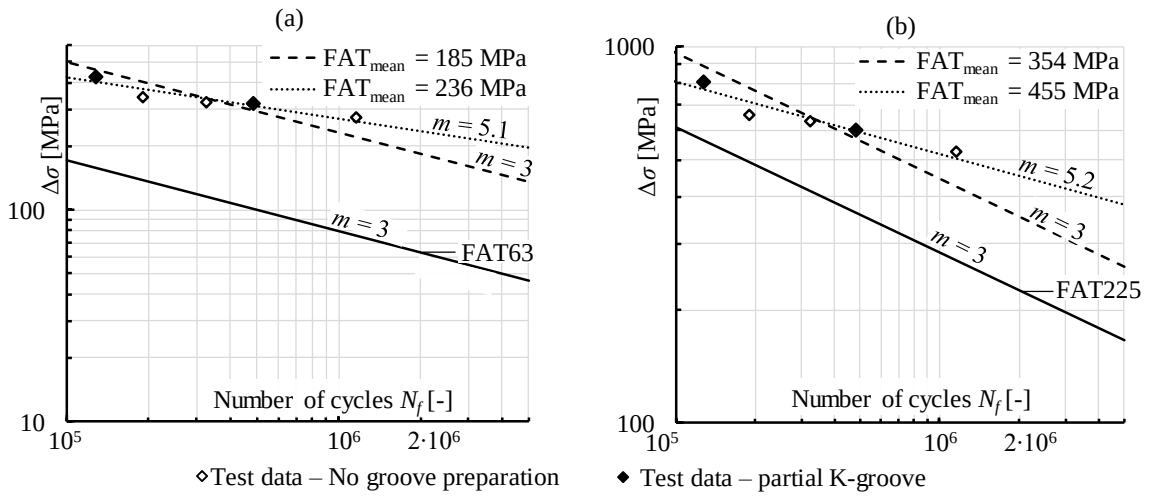

Fig. 7. Fatigue test results for bending loaded joints with toe failure and the derived S-N curves in terms of (a) NWS = HS stress, (b) ENS system.

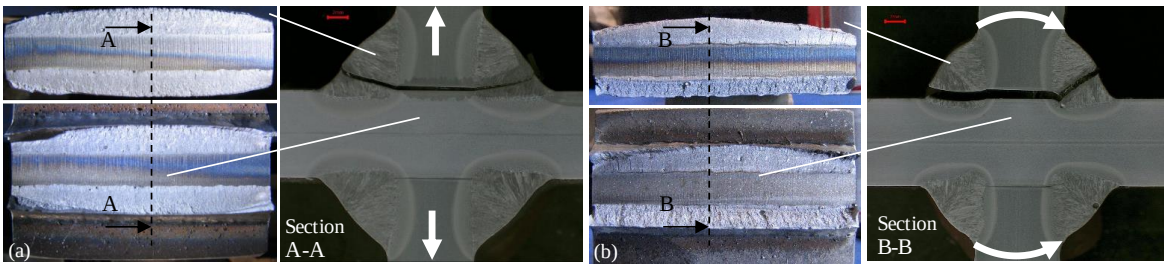

Fig. 8. Typical fracture surface and failure paths in (a) axially loaded joints (FWB_DYN17) and (b) bending loaded joints (FWB_DYN5).

3 NUMERICAL ANALYSIS

3.1 Computational fatigue capacity

Two-dimensional (2D) plane strain modeling was employed when computational fatigue strength capacities were obtained for the tested joints. The ENS concept and LEFM were applied in the analysis. Pre-processing and analysis of the ENS models were carried out using FEMAP/NxNastran v11.4.0 (Siemens PLM Software), and the crack propagation analysis and subsequent stress intensity factor (SIF), $\Delta K(a)$ evaluation was conducted using Casca/Franc2D v4 distributed by Cornell University [24]. The crack paths were calculated using maximum tangential stress criterion at the crack tip and SIFs were obtained utilizing the J-integral approach implemented in the Franc2D software. The geometry for each model was modeled following the measured geometry. The throat thicknesses and width of unpenetrated root gap were measured from the polished section at the center of the crack,

as presented in Section 2.4, Fig. 8. As shown in Fig. 8, neither excessive convexity nor concavity were found in the weldments, which could have affected the fatigue strength capacity. Consequently, the weld profile was simplified in terms of modeling only triangle-shaped geometry, as shown in Figs 9-10.

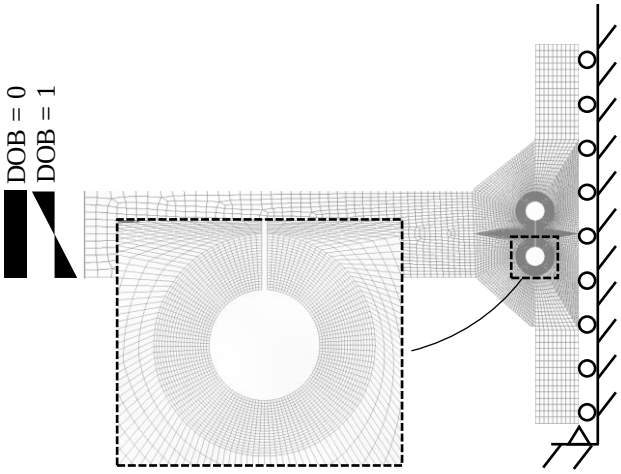

Fig. 9. ENS model with the reference radius of r_{ref} = 1.0 mm and showing the load and boundary conditions.

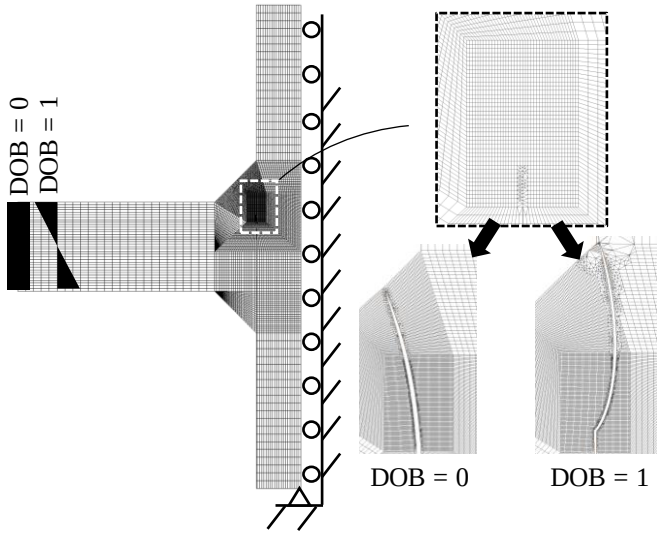

Fig. 10. Casca/Franc2D LEFM model with the initial and final cracks.

Fig. 11 illustrates the notch stress distribution along the circumference of the fictitious radius in terms of normalized stress and the maximum principal stress criterion (SCF = $\sigma_{max}/\sigma_{nom}$). The maximum values were used as representative SCFs in the fatigue strength assessment in the ENS concept, see Table 5 and Figs 6-7. In bending

loading, the maximum SCF = 0.73-0.81 was induced at approximately 100 degrees, i.e. 10 degrees from leg length section in the direction of the attached plate. In axial loading, the maximum SCF = 3.85-3.93 was at 80 degrees, i.e. 10 degrees from the leg length section in the direction of the weld reinforcement. The locations of the maximum SCFs correspond well to the directions of early crack propagation; see Fig. 8.

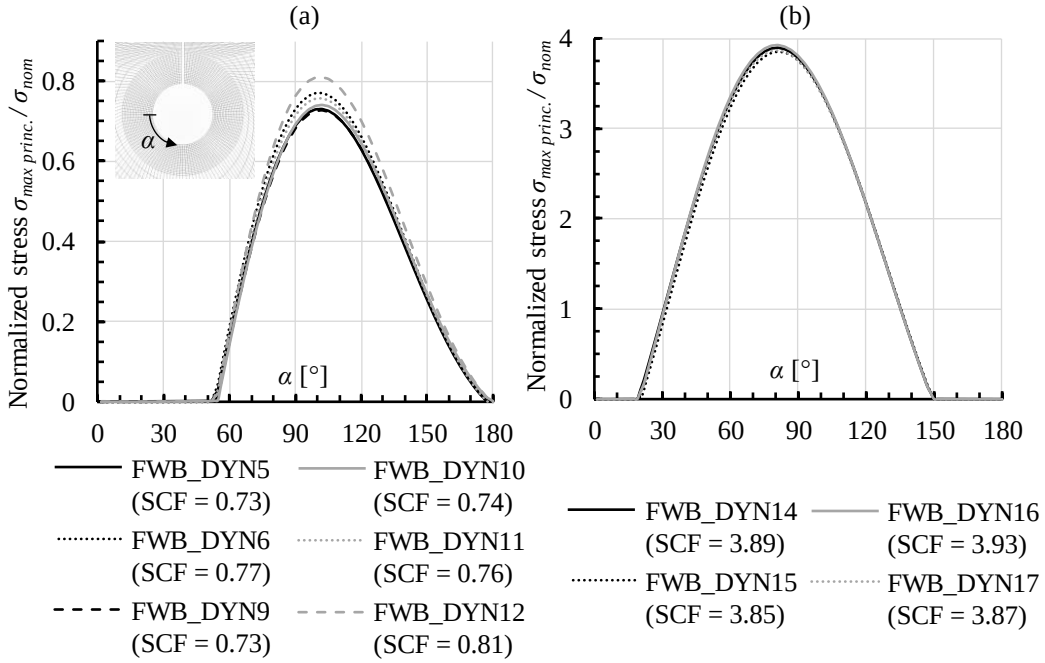

Fig. 11. Normalized stress along the circumference of fictitious notch radius, and the obtained SCFs for test specimens: (a) bending and (b) axially loaded joints.

Computational fatigue lives were obtained using mean S-N curves and the crack propagation coefficient (C_{mean}) for stress-based approaches and LEFM analyses, respectively. In the case of nominal stress and ENS approaches, mean S-N curves were obtained from characteristic design curves using safety factor of $j_\sigma = 1.37$ [25] representing the usual scatter bandwidth and failure probability of 2.3% (mean – 2Stdv). Thus, the computational mean fatigue strengths are 49 MPa (FAT36) for the nominal stress approach, and 308 MPa (FAT225) for the ENS concept. Paris' law and a numerical integrator were used when predicted fatigue life $N_{f,pred}$ was obtained using an LEFM-based analysis:

$$N_{f,pred} = \int_{a=a_i}^{a=a_f} \frac{da}{C \cdot \Delta K(a)^m} \tag{3}$$

Where a_i is the initial crack depth, a_f is the final crack depth, C is the crack propagation coefficient, $\Delta K(a)$ is the SIF range as a function of crack depth, and m is the slope of Paris' law. For the LEFM and subsequent fatigue life analysis, the mean values of crack propagation coefficients m and C were applied. Currently, the IIW Recommendations [4] propose $C_{char} = 5.21 \cdot 10^{-13}$ (da/dN in mm/cycle and ΔK in MPa·mm$^{1/2}$) , which was chosen as the reference crack propagation coefficient in this study. C_{mean} was obtained using the same ratio between C_{char} and C_{mean} as in [26,27], i.e. 3.0/1.7 = 1.76, resulting in $C_{mean} = 5.21 \cdot 10^{-13}/1.76 = 2.95 \cdot 10^{-13}$. In addition, the computational design fatigue lives were also obtained using the characteristic crack propagation coefficient. Fig. 12 presents the results for the computational fatigue lives with respect to the test results. Excluding one axially loaded test specimen (FWB_DYN15), the experimental fatigue life was higher than the predicted design fatigue life in all approaches. In general, the ENS system seems to be slightly unconservative, or there is no redundant safety with respect to the experimental test results. When using the LEFM or NWS system, there is no major difference between these approaches. Using LEFM and NWS, the predicted mean fatigue lives correspond quite well to the experimental test results, and on the other hand, design fatigue lives are distinctly lower compared with the experimentally obtained fatigue lives.

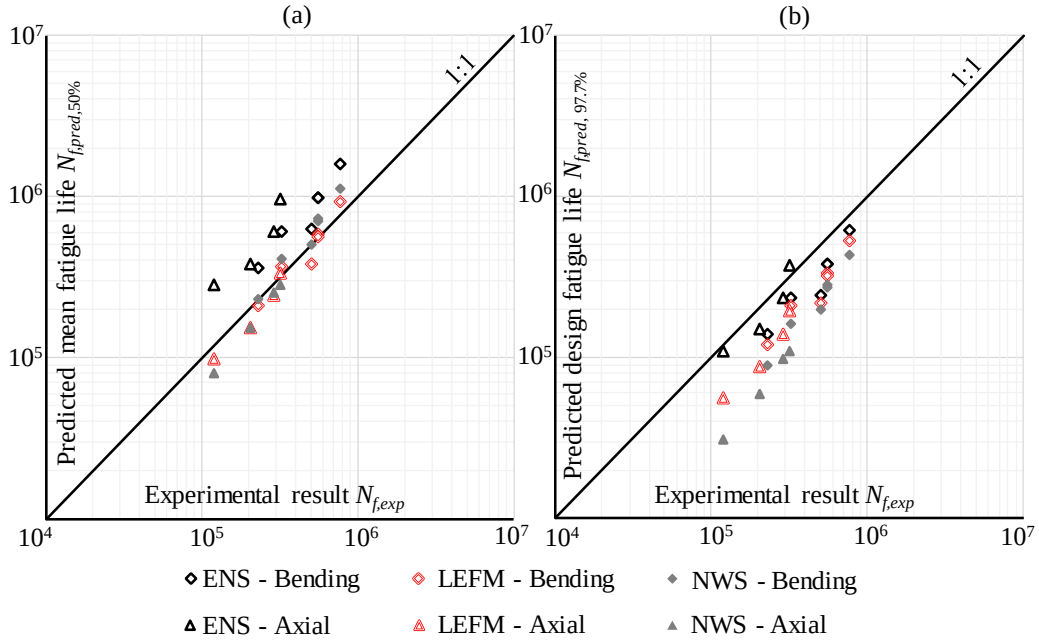

Fig. 12. Correlation between predicted fatigue life and experimental test result using (a) computational mean fatigue strength coefficients and (b) characteristic design coefficients in different fatigue strength assessment approaches.

3.2 Efficiency of weld penetration on improving fatigue strength capacity

Weld penetration plays an important role when assessing the weld root fatigue strength of LC joints. On the basis of the LEFM-based analysis, Maddox [28] showed that decreasing the infusible root face improves the weld root fatigue strength proportionally more than the weld toe capacity. However, previous studies have focused only on LC joints subjected to axial loading. Consequently, a parametric analysis on the effect of an increasing degree of weld penetration on the improvement level of the weld root fatigue strength capacity was carried out. The objective of this analysis was to investigate whether weld stress, see Eqs (1-2), should be calculated on the basis of effective throat thickness or leg length (external throat thickness summed with penetration length).

The analyses were conducted for a geometry corresponding to the tested specimens, i.e. a t = 9 mm LC joint with symmetric double-sided fillet welds. A total number of four different throat thicknesses were analyzed; a/t = 1/3, a/t = 1/2 and a/t = 2/3 with a flank angle of θ = 45°. Four different degrees of weld penetration were analyzed, focusing on the small degree of penetration, i.e. p/t = 0 (no penetration), p/t = 0.05, p/t = 0.1, p/t = 0.15 and p/t = 0.2 resulting in the total number of 30 LEFM analyses when both pure tensile and bending load conditions were considered. Otherwise, the model configuration, and boundary and load conditions were similar to the ones presented in Fig. 10. The improvement level was assessed relatively by comparing the fatigue strength capacity of the weld with penetration with welds without penetration as follows (LEFM data points in Figs 13-14):

$$k = \frac{FAT_{\text{penetrated}}}{FAT_{\text{fillet weld}}} = \frac{\left(\frac{N_{f,i}}{2\cdot 10^6}\right)^{\frac{1}{m}}\Delta\sigma}{\left(\frac{N_{f,p=0}}{2\cdot 10^6}\right)^{\frac{1}{m}}\Delta\sigma} = \frac{N_{f,i}^{\frac{1}{m}}}{N_{f,p=0}^{\frac{1}{m}}}, \tag{4}$$

where index i corresponds to the penetrated case $p = i$. In addition, the improvement level was assessed using Eqs (1-2) for axial and bending loading, respectively. Effective throat thickness a_{eff} (solid black line, Figs 13-14) and external throat thickness summed with penetration length, i.e. $a + p$ (dashed black line, Figs 13-14) were used as reference lengths for the fatigue strength assessment. In the axial loading, the fatigue strength capacity is linearly dependent on the length of the ligament (a_{eff} or $a + p$) but in the case of bending loading, the length of the ligament has a quadratic effect on the fatigue strength capacity; see Eqs (1-2).

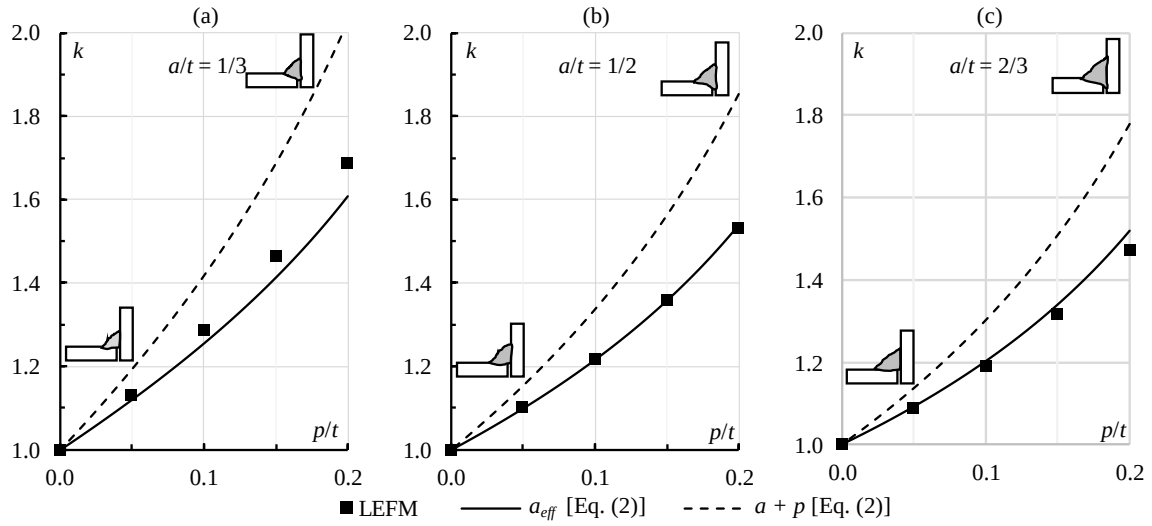

Fig. 13. Improvement level of weld root fatigue strength capacity in the bending loading using LEFM-based analysis for the different a/t ratios; (a) a/t = 1/3, (b) a/t = 1/2 and (c) a/t = 2/3.

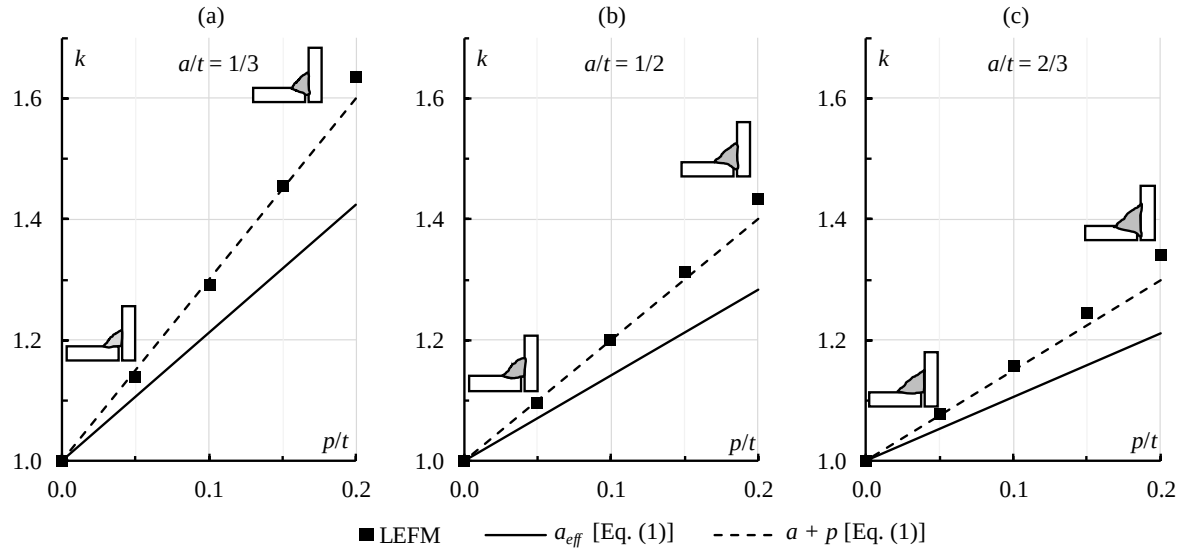

Fig. 14. Improvement level of weld root fatigue strength capacity in the axial loading using LEFM-based analysis for the different a/t ratios; (a) a/t = 1/3, (b) a/t = 1/2 and (c) a/t = 2/3.

4 DISCUSSION

In this study, the weld root fatigue strength capacity of double-sided fillet welds on steel plates subjected to out-of-plane bending was experimentally and numerically investigated. In the joints subjected to out-of-plane bending, nominal weld stresses were derived using linear-elastic stress distribution over the joint section, and the stress value at the non-propagated notch root (see Fig. 5 and Eq. (2)) was used as the basis for the calculation procedure.

In both the axial and bending load cases, effective throat thickness was used to consider the weld penetration in the tested joints. Using this approach, mean fatigue strengths of 47 MPa for bending loaded joints and 54 MPa for axially loaded joints, with the S-N curve slope of m =3, were acquired; see Fig. 6. Since a reasonable accordance in the fatigue strengths between the axially and bending loaded joints was achieved using a linear elastic stress distribution over the joint section, it can be proposed for design purposes. However, it must be recognized that this proposal is based on a limited number of test results, and further experimental verification should be conducted for various plate and throat thickness ratios and for other steel materials. It is also worth noting that the crack paths for the axial and bending loading vary, see Figs 8 and 10, and consequently, further experimental and numerical studies should be conducted considering different DOB ratios to see the combined effect of different load components on the root side fatigue strength capacity.

In terms of the ENS system, mean fatigue strengths computed separately for the axially and bending loaded joints (see Fig. 6b) exceeded the characteristic design curve FAT225. For bending loaded joints mean fatigue strength of 260 MPa was obtained, while for axially loaded joints, mean fatigue strength was 235 MPa. However, when considering the usual scatter in the design curves, the test results did not achieve the computed mean fatigue strength of 308 MPa (j_σ = 1.37) that has been also obtained for butt-welded joints with toe failure by Nykänen and Björk [29]. The unconservative nature of the use of the ENS concept for the fatigue strength assessment of root side failures has been exemplified in the previous works undertaken by Sundermeyer *et al*. [10] and Fricke and Kahl [11]. On the other hand, the weld root fatigue strength capacity is mainly associated with the gross ligament, i.e. throat thickness in fillet welds, and residual stress field at the weld root. Thus, the scatter in the test results is lower in the case of weld root failure than weld toe failure. However, since reasonably margin with respect to the FAT225 design curve was not found, a detailed scrutiny on the designed and realized weld throat thickness and penetration should be supervised.

In structural design and analysis, the weld penetration should be generally neglected unless a consistent weld penetration can be trustworthily achieved [30] and confirmed by non-destructive testing, such as radiographical or ultrasonic inspection. However, the consideration of weld penetration is of paramount importance when deriving the S-N curves since it significantly affects the obtained weld stress values. Further insight into the previous studies conducted in the field of weld root fatigue does not fully reveal whether the weld penetration was considered or weld stresses were calculated on the basis of external throat thickness. In this study, macrographic investigations, see Fig. 8 and Table 4, were conducted for each failed specimen to measure the length of the infusible weld root. These measures were used in the subsequent analyses to obtain analytical weld

stresses and to create finite element models for the ENS system and LEFM. In addition, a parametric analysis was conducted to investigate the effect of weld penetration on the root side fatigue strength capacity. This analysis revealed that in the case of bending loading, the improvement level corresponded to the analytical weld stress calculated on the basis of the effective throat thickness (a_{eff}), as shown in Fig. 13. Respectively, in the case of axial loading, the improvement level corresponded to the analytical weld stress calculated based on the external throat thickness summed with weld penetration; see Fig. 14. An explanatory factor for this issue has been presented in Fig. 15, in which the normalized stress distribution through the leg length section is plotted. The stress distributions were obtained from FE models of which detailed element meshes are shown in Fig. 15. Otherwise, the joint dimensions, and load and boundary conditions followed the models described in Figs 9-10. In the case of axial loading, the stress distribution is constantly decreasing through the leg length section while in the bending loading, a curved stress distribution can be seen and the top of the weld reinforcement near the weld toe does not sustain any significant load. Consequently, in the bending loading, the leg length is not fully effective near the weld toe, particularly when considering the analytical stress distribution shown in Fig. 5, and the weld root fatigue strength in the bending loading seems to correlate with the effective throat thickness.

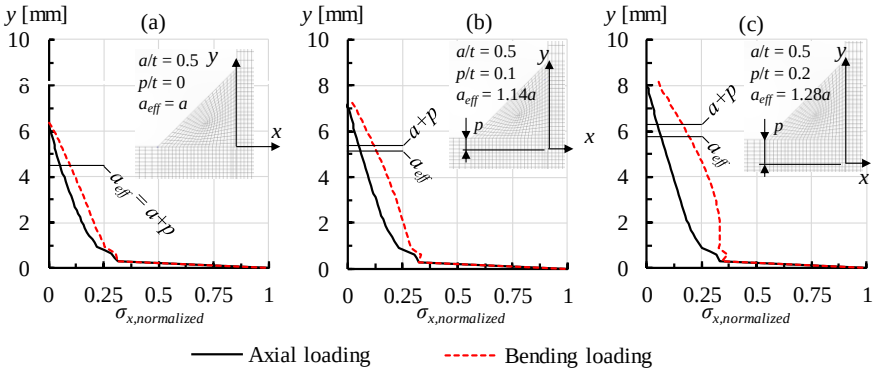

Fig. 15. Normalized normal stress ($\sigma_x/\sigma_{x,peak}$) distribution along the leg length section with different weld penetration lengths obtained by the FEA; (a) p/t = 0, (b) p/t = 0.1 and (c) p/t = 0.2.

Root side fatigue strength capacities were computed employing numerical methods. 2D plane strain models were used to obtain the SCFs for the ENS concept and the SIFs for the LEFM analysis. For a comparison, fatigue strength capacities were also obtained using an analytically determined NWS. Fig 12 shows the results of these analyses, indicating that both the analytical and LEFM analyses resulted in a good correspondence with the experimental results. When using characteristic design coefficients, a reasonable safety margin between the

characteristic design life (survival probability of 97.7%) and the experimental result was obtained. The ENS concept gave, again, unconservative results.

Within this study, the tests were carried out using the external stress ratio of $R = 0.1$, and the results are thus applicable for the joints subjected to the pulsating load conditions. Depending on the contact mechanism within the base plate and adjoined plate component, single-pass fillet weld may induce high compressive residual stress at the weld root [31,32], which makes the fatigue strength capacity susceptible to the external stress ratio. Nevertheless, for similar LC joints and filler materials used in this study, Ahola *et al.* [33] reported only 15% decrease in the weld root fatigue strength capacity when increasing the external stress ratio from $R = 0.1$ to $R = 0.5$. Due to these discrepancies, the further studies should pay attention to the formation of residual stress at the weld root in the UHSS materials, and to the effect of external stress ratio on the weld root fatigue strength capacity.

5 CONCLUSIONS

In the present paper, numerical and experimental analyses of the fatigue behavior of LC joints made of UHSS were carried out. According to the results of this study, the following conclusions can be drawn:

- Linear elastic stress distribution over the joint section can be used as a basis for the nominal weld stress (NWS) calculation for the bending loading. The characteristic FAT36 design curve for weld root failure, according to the design codes and guidelines [4–6], is applicable in this case.
- No significant improvement was found in the case of ultra-high-strength filler materials when weld root fatigue crack propagation was the critical design criterion. However, the FAT63 design curve for the toe failure in the bending loading was overly conservative. Furthermore, fatigue strength in terms of the ENS concept was very high in bending loading, whereby mean fatigue strength of 354 MPa ($m = 3$) was obtained for the joints failing from the weld toe. Plate bending stress induces a lower SCF than membrane stress; secondly, a stress gradient in the through thickness direction contributes to the achievement of a high fatigue strength.
- In bending, the fatigue strength improvement level at the weld root by increasing the weld penetration seems to correlate with the effective throat thickness, i.e. the shortest ligament, while in axial loading, the fatigue strength improvement seems to correlate with the external throat thickness summed with the weld penetration length.

- LEFM (C_{mean} = 2.95·10^{-13} √mm/MPa·cycle) and the NWS system (computational mean fatigue strength of 49 MPa) estimate the mean fatigue lives with a reasonable margin of error for both axial and bending loading. Respectively, considering the fatigue test results of this study and previous work on fillet welded joints, the ENS system gives unconservative fatigue life estimations for weld root failures.

ACKNOWLEDGEMENTS

This work was supported by Business Finland in the Digi-TuoTe project. In addition, the authors wish to thank M.Sc. (Tech.) Markus Haajanen for the significant contribution in the management of experimental testing.

REFERENCES

[1] Xing S, Dong P, Wang P. A quantitative weld sizing criterion for fatigue design of load-carrying fillet-welded connections. Int J Fatigue 2017;101:448–58. doi:10.1016/j.ijfatigue.2017.01.003.

[2] Cui C, Zhang Q, Bao Y, Kang J, Bu Y. Fatigue performance and evaluation of welded joints in steel truss bridges. J Constr Steel Res 2018;148:450–6. doi:10.1016/j.jcsr.2018.06.014.

[3] Singh PJ, Achar DRG, Guha B, Nordberg H. Fatigue life prediction of gas tungsten arc welded AISI 304L cruciform joints with different LOP sizes. Int J Fatigue 2002;25:1–7. doi:10.1016/S0142-1123(02)00067-1.

[4] Hobbacher A. Recommendations for Fatigue Design of Welded Joints and Components. 2nd ed. Cham: Springer International Publishing; 2016.

[5] EN 1993-1-9. Eurocode 3 - Design of steel structures - Part 1-9: Fatigue, 2005.

[6] DNVGL-RP-C203. Fatigue Design of Offshore Steel Structures, 2016.

[7] Fricke W, Kahl A, Paetzold H. Fatigue Assessment of Root Cracking of Fillet Welds Subject To Throat Bending Using the Structural Stress Approach Fatigue Assessment of Root Cracking of Fillet Welds Subject To Throat Bending Using the Structural Stress Approach for Structural Stress. Weld World 2006;50:64–74. doi:10.1007/BF03266538.

[8] Sørensen JD, Tychsen J, Andersen JU, Brandstrup RD. Fatigue Analysis of Load-Carrying Fillet Welds. J Offshore Mech Arct Eng 2006;128:65. doi:10.1115/1.2163876.

[9] Sonsino CM, Fricke W, De Bruyne F, Hoppe A, Ahmadi A, Zhang G. Notch stress concepts for the fatigue assessment of welded joints - Background and applications. Int J Fatigue 2012;34:2–16. doi:10.1016/j.ijfatigue.2010.04.011.

[10] Sundermeyer W, Fricke W, Paetzold H. Investigation of weld root fatigue of single-sided welded T-joints. In: Soares Guedes C, Shenoi RA, editors. Anal. Des. Mar. Struct. V, London: Taylor & Francis Group; 2015, p. 309–15.

[11] Fricke W, Kahl A. Fatigue assessment of weld root failure of hollow section joints by structural and notch stress approaches. In: Packer JA, Willibald S, editors. Proc. 11th Int. Conf. Tubul. Struct., 2006, p. 593–600.

[12] Kim IT, Kainuma S. Fatigue life assessment of load-carrying fillet-welded cruciform joints inclined to uniaxial cyclic loading. Int J Press Vessel Pip 2005;82:807–13. doi:10.1016/j.ijpvp.2005.07.004.

[13] Khurshid M, Barsoum Z, Däuwel T, Barsoum I. Root fatigue strength assessment of fillet welded tube-to-plate joints subjected to multi-axial stress state using stress based local methods. Int J Fatigue 2017;101:209–23. doi:10.1016/j.ijfatigue.2017.02.007.

[14] Frendo F, Bertini L. Fatigue resistance of pipe-to-plate welded joint under in-phase and out-of-phase combined bending and torsion. Int J Fatigue 2015;79:46–53. doi:10.1016/j.ijfatigue.2015.04.020.

[15] Gurney TR, MacDonald K. Literature Survey on Fatigue Strengths of Load-Carrying Fillet Welded Joints Failing in the Weld. Report OTH 91 356. 1995.

[16] Jakubczak H, Glinka G. Fatigue analysis of manufacturing defects in weldments. Int J Fatigue 1986;8:51–7.

[17] Song W, Liu X, Razavi SMJ. Fatigue assessment of steel load-carrying cruciform welded joints by means of local approaches. Fatigue Fract Eng Mater Struct 2018:1–16. doi:10.1111/ffe.12870.

[18] Radaj D, Helmers K. Bewertung von Scheißverwindungen hinsichtlich Schwingfestingkeit nach dem Kerbspannungskonzept (in German). Konstruktion 1997;49:21–7.

[19] Lie ST, Lan S. A boundary element analysis of misaligned load-carrying cruciform welded joints. Int J Fatigue 1998;20:433–9. doi:10.1016/S0142-1123(97)00133-3.

[20] Kang W, Kim WS, Paik YM. Fatigue strength of fillet welded steel structure under out-of-plane bending. Int J Korean Weld Soc 2002;2:33–9.

[21] EN ISO 4063. Welding and allied processes. Nomenclature of processes and reference numbers (Corrected version 2010-03-01)., 2018.

[22] EN 1011-1. Welding - Recommendations for welding of metallic materials - Part 1: General quidance for arc welding, 2009.

[23] BS7608:2014 +A1:2015. Guide to Fatigue Design and Assessment of Steel Products, 2015.

[24] Cornell University. Software 2018. http://cfg.cornell.edu/software/ (accessed October 23, 2018).

[25] Radaj D, Sonsino CM, Fricke W. Fatigue Assessment of Welded Joints by Local Approaches. 2nd editio. Cambridge: Woodhead Publishing; 2006.

[26] Lohne P. A fracture mechanics approach to fatigue analysis of welded joints in offshore structures. J Nor Marit Res 1979;7:12–20.

[27] King RN, Stacey A, Sharp J V. A review of fatigue crack growth rates for offshore steels in air and seawater environments. In: Mercati D, editor. Proc. 15th Int. Conf. Offshore Mech. Arct. Eng. OMAE, 1996, p. 341–8.

[28] Maddox S. Assessing the significance of flaws in welds subject to fatigue. Weld J 1974;53:401–10.

[29] Nykänen T, Björk T. Assessment of fatigue strength of steel butt-welded joints in as-welded condition - Alternative approaches for curve fitting and mean stress effect analysis. Mar Struct 2015;44:288–310. doi:10.1016/j.marstruc.2015.09.005.

[30] EN 1993-1-8. Eurocode 3 - Design of steel structures - Part 1-8: Design of joints, 2005.

[31] Mori T, Ichimiya M. Fatigue crack initiation point in load carrying fillet-welded cruciform joints. Weld Int 1999;10:786–94.

[32] Barsoum Z, Lundbäck A. Simplified FE welding simulation of fillet welds - 3D effects on the formation residual stresses. Eng Fail Anal 2009;16:2281–9. doi:10.1016/j.engfailanal.2009.03.018.

[33] Ahola A, Skriko T, Björk T. Experimental investigation on the fatigue strength assessment of welded joints made of S1100 ultra-high-strength steel in as-welded and post-weld treated condition (in press). In: Zingoni A, editor. Proc. 7th Int. Conf. Struct. Eng. Mech. Comput. Cape Town, South Africa, 2-4 Sept. 2019, 2019, p. 1–6.